Force rebalance control for a MEMS gyroscope using ascending frequency drive and generalized PI control

Chun-Hua HE[1,2], Qin-Wen HUANG[2], Qian-Cheng ZHAO[1], Zhen-Chuan YANG[1] , Da-Cheng ZHANG[1] and Gui-Zhen YAN[1]

[1]*National Key Laboratory of Science and Technology on Micro/Nano Fabrication, Institute of Microelectronics, Peking University, Beijing 100871, P. R. China*

[2]*Science and Technology on Reliability Physics and Application of Electronic Component Laboratory, No.5 Electronics Research Institute of the Ministry of Industry and Information Technology, Guangzhou, 510610, Guangdong, P. R. China*

Abstract. This paper has proposed a novel force rebalance control method for a MEMS gyroscope using ascending frequency drive and generalized PI control. Theoretical analyses of ascending frequency drive and force rebalance control methods are illustrated in detail. Experimental results demonstrate that the electrical anti-resonant peaks are located at the frequency responses in the RFD system, which seriously deteriorates the original response characteristics. However, they are eliminated in the AFD system, and the electrical coupling signal is also suppressed. Besides, as for the force rebalance control system, the phase margins approximate to 60deg, gain margins are larger than 13dB, and sensitivity margins are smaller than 3.2dB, which validates the control system is stable and robust. The bandwidth of the force rebalance control system is measured to be about 103.2Hz, which accords with the simulation result. The bias instability and angle random walk are evaluated to be 1.65deg/h and 0.06deg/√h, respectively, which achieves the tactical level.

Keywords: MEMS gyroscope, mode-matching, force rebalance control, ascending frequency drive, electrical coupling suppressing.

Introduction

Electrical coupling is one of the major error sources for a MEMS gyroscope, which is induced by the direct coupling from the drive combs to the sense combs through the parasitic capacitances [1-2]. It will bring about the non-ideal anti-resonance at the amplitude-frequency responses of drive mode and sense mode, which deteriorates the performance and affects the reliability of the closed loop system. Therefore, it is significant to suppress the electrical coupling signals by modifying the control and readout circuit. Electromechanical amplitude modulation (EAM) [3] method can modulate the actual vibration signal by exerting a high-frequency carrier (usually several MHz) to the public mass. Thus, coupling signals can be separated and eliminated from the useful sense signal easily. However, a demodulation process should be added to restore the useful information, which will complicate the control system. Furthermore, the circuit has to handle the demodulation in high frequency domain, which increases the hardware cost, power consumption and high frequency noise.

By introducing a drive modulation process, ascending frequency drive (AFD) method [4-5] is proved effective to suppress the electrical coupling for the drive mode of a MEMS gyroscope. Compared with EAM, it can simplify the readout circuit since it needs no extra demodulation process. In addition, compared to resonant frequency drive (RFD) method, the noise in AFD system can be further suppressed. Hence, in this paper, AFD method will be applied to the force rebalance control system for sense mode of a MEMS gyroscope. Nowadays, force rebalance control for the sense mode is widely adopted in high-performance gyroscopes, since it can adjust the bandwidth, improve the nonlinearity, extend the measure range [6-9]. As for EAM

method, a lot of researches about the force rebalance control have been fulfilled and reported in our previous work [8-9]. In this work, novel theoretical analysis of force rebalance control with AFD method will be conducted in detail.

Theoretical analysis

Electrical coupling suppressing

The simplified schematic of a Z-axis doubly decoupled MEMS tuning fork gyroscope is shown in Fig. 1 (a). It mainly includes drive combs, drive-sensing combs, sense combs, force feedback combs, and mode-matching combs. The key parameters of the tested gyroscope at room temperature are listed in Table 1. The resonant frequency of the sense mode ω_s will equal the resonant frequency of the drive mode ω_d after mode-matching control. Fig. 1 (b) shows that there are some parasitic capacitances between the drive combs and sense combs since they are close to each other in the layout.

Table 1. Key parameters of the tested gyroscope at room temperature.

Parameter	Value
Drive mode resonant frequency f_d	9451.5Hz
Drive mode quality factor Q_d	11385
Sense mode resonant frequency f_s	9481.1Hz
Sense mode quality factor Q_s	2300

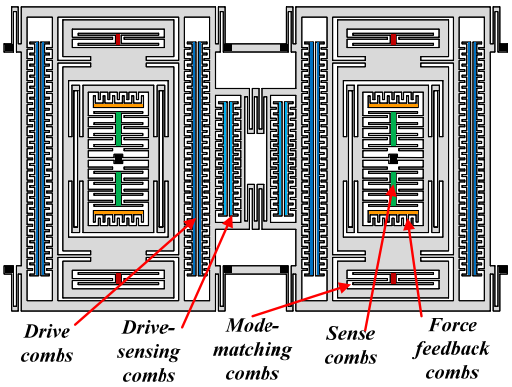

(a) The simplified schematic of a Z-axis doubly decoupled MEMS tuning fork gyroscope

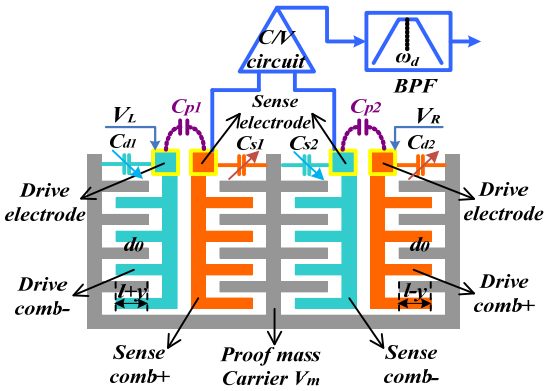

(b) Electrical coupling analysis between the drive combs and sense combs of a MEMS gyroscope

Fig. 1. Electrical coupling analysis of a MEMS gyroscope.

In order to fulfill the differential detection, a *DC* carrier signal V_m is exerted to the proof mass. C_{d1} and C_{d2} are the differential drive capacitances, while C_{s1} and C_{s2} are the differential sense capacitances. C_{p1} and C_{p2} stand for the differential parasitic capacitances between the drive combs and sense combs. V_L and V_R represent the two differential drive signals. Owing to the existence of parasitic capacitances, drive signals can be coupled to the sense combs, which will disturb the original detection signal and deteriorate the closed loop system's stability and performance. Fig. 2 and Fig. 3 depict the schematics of the readout circuit and AFD circuit for the sense mode of a MEMS gyroscope, respectively. In the readout circuit, the output of differential amplifier can be derived as:

$$V_{out} = \frac{k_g[V_m(C_{s2}-C_{s1})+(V_R C_{p2}-V_L C_{p1})]}{C_f} \quad (1)$$

Where, k_g is the gain of the differential amplifier, and C_f is the feedback capacitance of the charge amplifier. In the RFD circuit, the frequencies of V_L and V_R equals to those of C_{s1} and C_{s2}, thus it is hard to distinguish $V_m(C_{s2}-C_{s1})$ from $(V_R C_{p2}-V_L C_{p1})$. Due to the influence of coupling signal, there will be a non-ideal anti-resonance appeared at the amplitude-frequency response [4-5]. However, in the AFD circuit, the frequency of V_L and V_R is far larger than that of C_{s1} and C_{s2}, thus the coupling signal $(V_R C_{p2}-V_L C_{p1})$ can be eliminated by a suitable band-pass-filter (BPF).

Therefore, after filtered by BPF, y_{out} can be described as:

$$y_{out} = \frac{k_g V_m (C_{s2} - C_{s1})}{C_f} = \frac{2k_g V_m N_s \varepsilon h}{C_f d_0} y \quad (2)$$

Where, y is the displacement of the sense mode, ε is the permittivity, N_s is the number of sense capacitances, h is the thickness, and d_0 is the gap. From equation (2), the gain k_{cv} of the readout circuit can be obtained as:

$$k_{cv} = \frac{2k_g V_m N_s \varepsilon h}{C_f d_0} \quad (3)$$

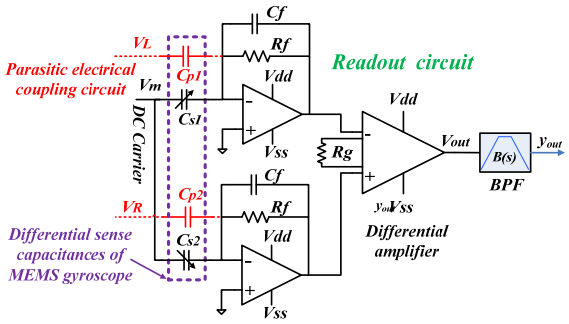

Fig. 2. The readout circuit for the sense mode of a MEMS gyroscope.

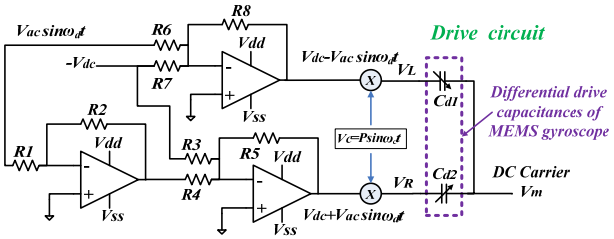

Fig. 3. AFD circuit for the sense mode of a MEMS gyroscope.

From Fig. 3, V_L and V_R can be yielded as:

$$V_R = (V_{dc} + V_{ac}\sin(\omega_d t))P\sin(\omega_c t) \quad (4)$$

$$V_L = (V_{dc} - V_{ac}\sin(\omega_d t))P\sin(\omega_c t) \quad (5)$$

Where, V_{dc} and $V_{ac}sin(\omega_d t)$ are the DC and AC drive signals. $Psin(\omega_c t)$ is the high frequency carrier, and ω_c ? ω_d . Take the noises n_1 and n_2 into account, the drive signals V_1 and V_2 of the differential drive capacitances can be derived as:

$$V_2 = V_R - V_m + n_2 = (V_{dc} + V_{ac}\sin(\omega_d t))P\sin(\omega_c t) - V_m + n_2 \quad (6)$$

$$V_1 = V_L - V_m + n_1 = (V_{dc} - V_{ac}\sin(\omega_d t))P\sin(\omega_c t) - V_m + n_1 \quad (7)$$

From Fig. 1 (b), the energies of the differential drive capacitances can be expressed as:

$$E_2 = \frac{NV_2^2 \varepsilon h(l - y)}{d_0} \quad (8)$$

$$E_1 = \frac{NV_1^2 \varepsilon h(l + y)}{d_0} \quad (9)$$

Where, N is the number of drive capacitances, and l is the overlapped length. Then, the total drive force can be derived as:

$$F_{tot} = \frac{-\partial E_1}{\partial y} + \frac{-\partial E_2}{\partial y} = \frac{N\varepsilon h(V_2^2 - V_1^2)}{d_0} = \frac{N\varepsilon h}{d_0}[2P^2 V_{dc} V_{ac}\sin(\omega_d t) + (n_2 + n_1 - 2V_m)(n_2 - n_1)$$
$$-2P^2 V_{ac} V_{dc}\sin(\omega_d t)\cos(2\omega_c t) + 2(n_2 - n_1)V_{dc} P\sin(\omega_c t) + 2(n_2 + n_1 - 2V_m)V_{ac} P\sin(\omega_d t)\sin(\omega_c t)] \quad (10)$$

Since the frequency response of a gyroscope can be regarded as a BPF, the lower and higher frequency components will be suppressed, and the real useful force can be yielded as:

$$F_{useful} = \frac{2N\varepsilon h P^2 V_{dc}}{d_0} V_{ac}\sin(\omega_d t) \quad (11)$$

Equation (11) indicates that the noises can be suppressed, and there is no need to demodulate the readout signal y_{out} since the frequency of y is ω_d, rather than $\omega_c \pm \omega_d$. Hence, the gain k_{vf} of the drive circuit can be expressed as:

$$k_{vf} = \frac{2N\varepsilon h P^2 V_{dc}}{d_0} \quad (12)$$

Force rebalance control

AFD method is effective to suppress the coupling signal, which is detailedly illustrated above. k_{cv} and k_{vf} of the AFD circuit are yielded in equations (3) and (12). Thus the force

rebalance control system for the sense mode can be introduced as Fig. 4. Where, $-\Omega(t)$ and $q(t)$ are input angular rate and quadrature coupling signal, respectively. F_c, F_q and F_b represent Coriolis force, quadrature force, and feedback force, respectively. m_pA_v, k_{qf} and k_{vf} are corresponding force coefficients of them. m_s and m_p represent the sense mass and proof mass, respectively. A_v stands for the amplitude of the drive velocity. k_{dc} is the conversion coefficient from displacement to capacitance, and θ is the demodulation phase. The transfer functions of the sense mode $G_s(s)$, BPF $B(s)$, low-pass-filter (LPF) $L(s)$, and generalized-PI (G-PI) controller $P(s)$ are defined as follows:

$$G_s(s)=\frac{k_{dc}/m_s}{s^2+s\omega_s/Q_s+\omega_s^2} \tag{13}$$

$$B(s)=\frac{2\xi_b\omega_b s}{s^2+2\xi_b\omega_b s+\omega_b^2} \tag{14}$$

$$L(s)=\frac{\omega_l^2}{s^2+2\xi_l\omega_l s+\omega_l^2} \tag{15}$$

$$P(s)=\frac{k_p(s+\omega_2)}{(s+\omega_1)(s+\omega_3)} \tag{16}$$

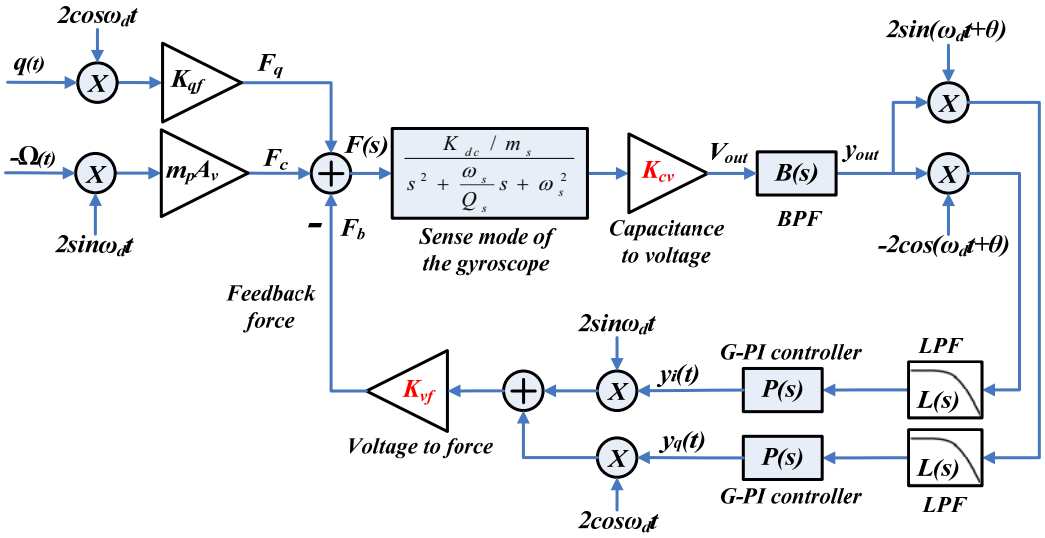

Fig. 4. Force rebalance control system with AFD method for the sense mode of a MEMS gyroscope.

Where, ξ_b and ω_b are the damping ratio and centre frequency of BPF, ξ_l and ω_l are the damping ratio and cut-off frequency of LPF, k_p, ω_1, ω_2 and ω_3 are the key parameters of G-PI controller. There are two control loops shown in Fig. 4, one is utilized to rebalance the Coriolis force, while another is used to rebalance the quadrature force. As for this force control system, the transfer function of the open loop system $D(s)$ can be deducted easily based on Fig. 4:

$$D(\mathrm{s})=\frac{F_b(s)}{F(s)}=2jk_{cv}k_{vf}[e^{-j\theta}L(j\omega-j\omega_d)P(j\omega-j\omega_d)-e^{j\theta}L(j\omega+j\omega_d)P(j\omega+j\omega_d)]B(j\omega)G_s(j\omega) \tag{17}$$

Where, complex frequency s is equal to $j\omega$. Thus the transfer function of the closed loop system $T(s)$ and the sensitivity function $S(s)$ can be yielded as:

$$T(s)=\frac{D(s)}{1+D(s)} \tag{18}$$

$$S(s)=\frac{1}{1+D(s)} \tag{19}$$

Experimental test

Swept frequency test

The simplified schematic of a Z-axis doubly decoupled MEMS tuning fork gyroscope is shown in Fig. 5. It mainly includes an analog circuit and a digital circuit. Swept frequency tests of the sense mode are conducted in the RFD system and AFD system, respectively. Experimental results demonstrate that the electrical anti-resonant peaks are located at the amplitude-frequency and phase-frequency responses in the RFD system, which seriously deteriorates the original response characteristics, as shown in Fig. 6 (a). Due to the existence of electrical anti-resonant peaks, it is very hard to design a suitable G-PI controller to guarantee the reliability and robustness of the force rebalance control system. Therefore, it is urgent to suppress the electrical coupling. On the other hand, in Fig. 6 (b), there are no anti-resonant peaks appeared in the AFD system, and the electrical coupling signal is eliminated, which indicates the theoretical analysis is accurate.

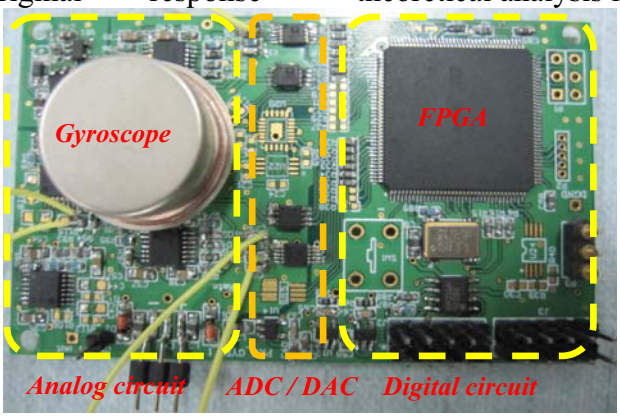

Fig. 5. The simplified schematic of a Z-axis doubly decoupled MEMS tuning fork gyroscope.

Force rebalance control test

After the theoretical deduction above, equations (3) and (12)-(19) can be utilized to design the closed loop system. Simultaneously, simulations based on these equations are accomplished with Matlab software, as shown in Fig. 7 and Fig. 8. In Fig. 7, owing to narrow-band force rebalance control, there are two crossover frequencies appearing in the frequency-amplitude response of $D(s)$. Thus, similar to our previous analysis [9], there are two corresponding phase margins (PM_l and PM_r), gain margins (GM_l and GM_r), cut-off frequencies (f_{tl} and f_{tr}) and sensitivity margins (M_{sl} and M_{sr}), as marked in the figure. The key stability indices of the feedback control system obtained by Matlab simulation are listed in Table 2. According to classical linear control theory, the force rebalance control system is stable and robust enough. Besides, the bandwidth (BW_{lr}) of $T(s)$ is calculated to be 103.18Hz, which means the force outside this narrow-band will never be balanced.

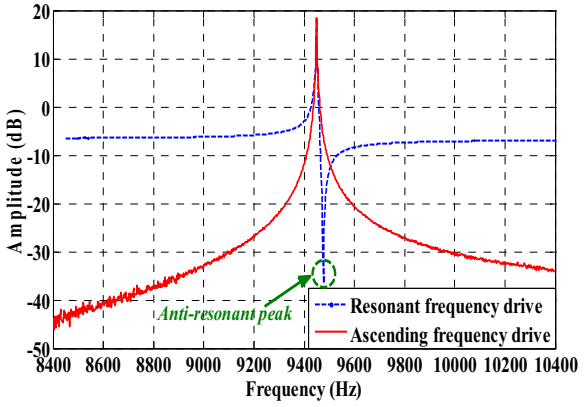

(a) Amplitude-frequency response

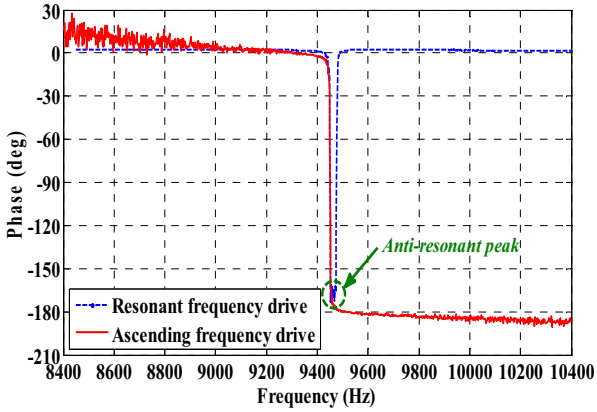

(b) Phase-frequency response

Fig. 6. Swept frequency tests of the sense mode in RFD and AFD methods.

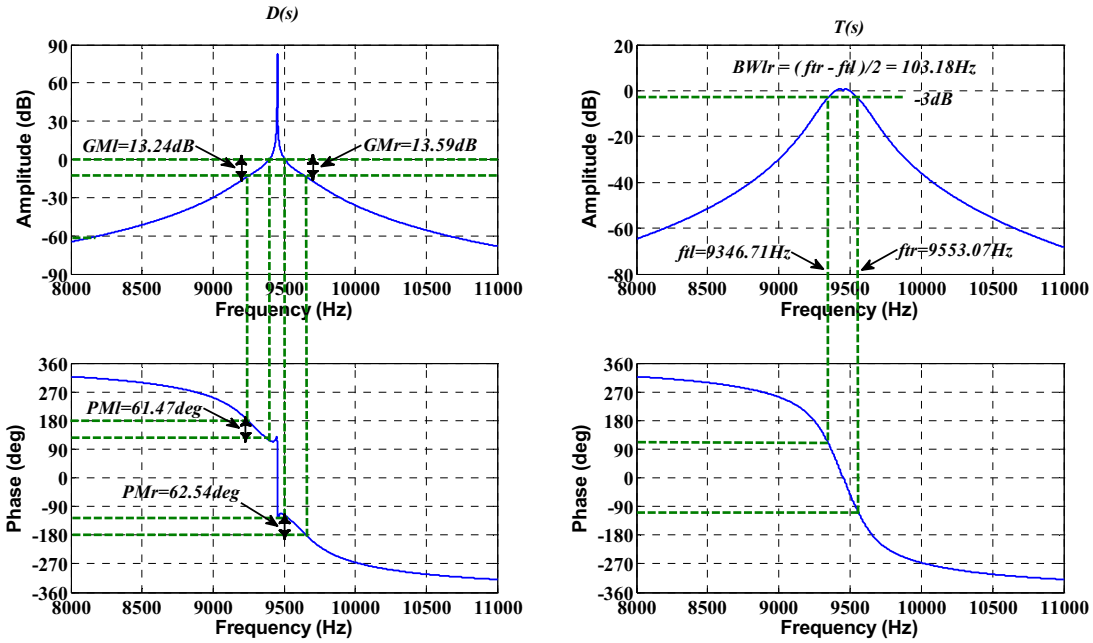

Fig. 7. The frequency responses of the open loop system *D(s)* and closed loop system *T(s)*.

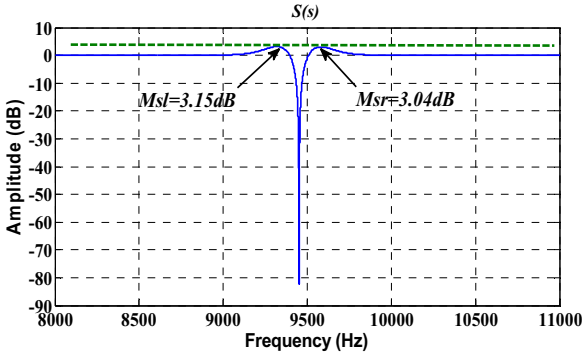

Fig. 8. The frequency response of the sensitivity function *S(s)*.

Table 2. Key stability indices of the feedback control system obtained by Matlab simulation.

Type	Key stability indices	
Phase margin PM (deg)	PM_l=61.47	PM_r=62.54
Gain margin GM (dB)	GM_l=13.24	GM_r=13.59
Sensitivity margin Ms (dB)	M_{sl} =3.15	M_{sr}=3.04
Cut-off frequency f_t (Hz)	f_{tl}=9346.71	f_{tr}=9553.07
Bandwidth BW (Hz)	BW_{lr} =(f_{tr} - f_{tl})/2=103.18Hz	

The bandwidth (BW) of the force rebalance control system is measured to be about 103.2Hz, which approximates to the simulation result, as shown in Fig. 9. It further verifies the theoretical analysis of the closed loop system is precise. The scale factor of the MEMS gyroscope with closed loop controlled sense mode is 65.9mV/deg/s with nonlinearity of 0.03%. Fig. 10 illustrates that the bias instability and angle random walk are evaluated to be 1.65deg/h and 0.06deg/√h, respectively, which reaches the tactical level.

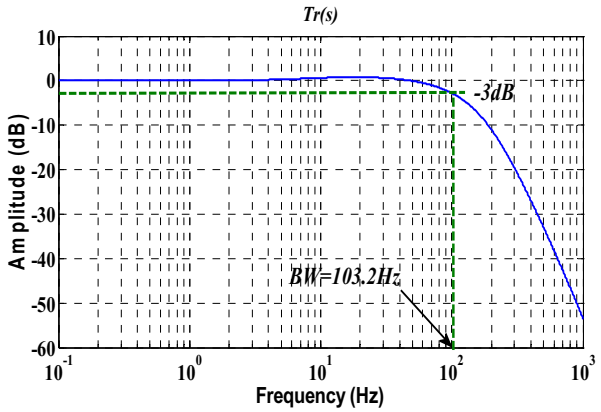

Fig. 9. Bandwidth test results of the closed loop control system.

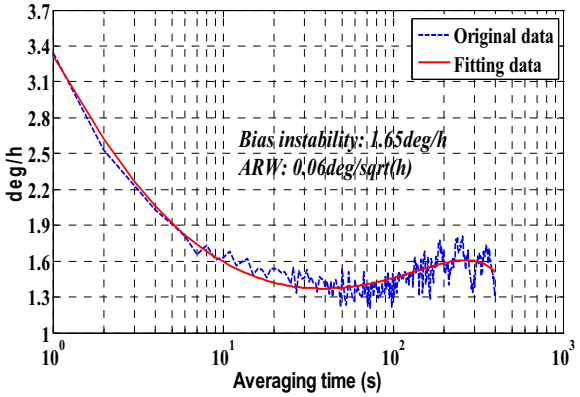

Fig. 10. Allan variance graph of bias drift of the MEMS gyroscope with closed loop controlled sense mode.

Summary

In this paper, a novel force rebalance control method has been presented for a MEMS gyroscope using ascending frequency drive and generalized PI control. Theoretical analyses of ascending frequency drive and force rebalance control methods are illustrated in detail. Experimental results demonstrate that the electrical anti-resonant peaks are located at the amplitude-frequency and phase-frequency responses in the RFD system, which seriously deteriorates the original response characteristics. However, they are eliminated in the AFD system, and the electrical coupling signal is also suppressed. On the other hand, the frequency responses of the force rebalance control system indicate that the phase margins approximate to 60deg, gain margins are larger than 13dB, and sensitivity margins are smaller than 3.2dB, which validates the control system is stable and robust. The bandwidth of the force rebalance control system is measured to be about 103.2Hz, which verifies the theoretical analysis is accurate. The bias instability and angle random walk are evaluated to be 1.65deg/h and 0.06deg/√h, respectively, which reaches the tactical level.

Acknowledgement

This work is partially supported by the National Natural Science Foundation of China under Grant No. 61434003.

References

[1] Lee, H. Ko, et al., “Non-ideal behavior of a driving resonator loop in a vibratory capacitive microgyroscope”, Microelectronics J., vol. 39, 2008, pp. 1-6.

[2] M.S. Weinberg and A. Kourepenis, “Error sources in in-plane silicon tuning-fork MEMS gyroscopes”, J. Microelectromech. Syst., vol. 15, 2006, pp. 479-491.

[3] Acar, A.M. Shkel, “Structurally decoupled micromachined gyroscopes with post-release capacitance enhancement”, J. Micromech. Microeng., 2005, 15 1092-1101.

[4] J. Cui, Z. Y. Guo, Z.C. Yang, et al., “Electrical coupling suppressing for a microgyroscope using ascending frequency drive with 2-DOF PID controller”, Proc. Transducers 2011, pp. 2002-2005.

[5] J. Cui, Z.Y. Guo, Z.C. Yang, et al., “Electrical coupling suppression and transient response improvement for a microgyroscope using ascending frequency drive with a 2-DOF PID controller”, J. Micromech. Microeng., 2011, 21 095020.

[6] S. Sonmezoglu, S.E. Alper, T. Akin, “An Automatically Mode-Matched MEMS Gyroscope With Wide and Tunable Bandwidth”, J. Microelectromech. Syst., Vol. 23, No. 2, 2014, pp.284-297.

[7] R. Mirjalili, H. Wen, D. E. Serrano, and F. Ayazi, “Substrate-decoupled silicon disk resonant having degenerate gyroscopic

modes with Qin excess of 1-million", Proc. TRANSDUCERS 2015, pp. 15-18.

[8] C.H. He, Q.C. Zhao, Y.X. Liu, et al., "Closed loop control design for the sense mode of micromachined vibratory gyroscopes", Sci. China Tech. Sci. 2013, Vol. 56, pp. 1112-1118.

[9] C.H. He, D.C. Liu, Q.C. Zhao, et al., "A novel narrow-band force rebalance control method for the sense mode of MEMS vibratory gyroscopes", Measurement, vol. 62, 2015, pp. 197-204.